JCTC Journal of Chemical Theory and Computation

Letter

pubs.acs.org/JCTC

Exploring the Reaction Coordinates for f–f Emission and Quenching of Lanthanide Complexes – Thermosensitivity of Terbium(III) Luminescence

Miho Hatanaka* and Keiji Morokuma*

Fukui Institute for Fundamental Chemistry, Kyoto University, Kyoto, 606-8103 Kyoto, Japan

Supporting Information

ABSTRACT: Lanthanide complexes with temperature dependent f–f emission intensities are commonly used as temperature sensors. The thermosensitivity can be controlled by the ligands, but their effects are difficult to predict. To clarify the origin of the differences in thermosensitivity, we propose a new theoretical strategy, the energy shift method, and use it to find crossing points between two states where intersystem crossing and excitation energy transfer take place. The different sensitivities of the three studied terbium(III) complexes are caused by the different rate-determining steps for emission or quenching.

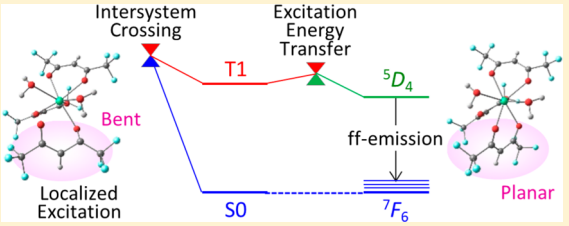

Intra $4f^N$ transitions (f–f transitions) of lanthanide (Ln) complexes have been widely used as luminescence probes.[1−3] Some of the advantages of the f–f transitions in Ln^{3+} probes are that the shapes of the emission spectra are very sharp, the emission wavelengths are independent of the environment, and only the emission intensities are sensitive to the surroundings.[4,5] These can be explained by the character of 4f electrons. Open-shell 4f electrons of Ln^{3+} are shielded from the environment by the closed-shell 5s and 5p electrons. Therefore, the excitation energies of $4f^N$ excited states are independent of the surroundings. For the same reason, the shapes of the potential energy surfaces (PESs) of $4f^N$ states for a given N are almost the same,[4,5] and only the f–f transitions between the vibronic states with the same vibrational quantum numbers are allowed, which results in the sharp peaks of f–f transitions.[6,7] The $4f^N$ electronic states of Ln^{3+} complexes are typically denoted by ^SL_J of the isolated Ln^{3+} cation because the crystal field splittings caused by the ligands are smaller than the spin–orbit splittings.[1−7] The excitations of Ln^{3+} complexes are localized either on Ln^{3+} or on the ligands because of the negligibly small overlap of 4f orbitals with the ligand orbitals; thus, the electronic states of these complexes can be denoted by (Sn, ^SL_J), where Sn and ^SL_J are the localized electronic states of the ligands and Ln^{3+}, respectively.

An interesting application of Ln complexes is in thermosensitive luminescent probes that use Eu^{3+} and Tb^{3+}.[8−16] Tb^{3+} complexes show green emissions caused by the f–f transitions from $^5D_4$ to ^7F_J (J = 6–0). With appropriate ligands, the intensity of the green emission decreases as temperature increases, enabling these complexes to be used as temperature sensors. Generally, the mechanism of Tb^{3+} luminescence has been explained by five steps, as shown in Figure 1.[3,17−20] The process starts from (1) ligand-centered excitation from the singlet ground state (S0) to a singlet excited state (Sn), followed by (2) intersystem crossing (ISC) from Sn to the lowest triplet state (T1), (3) excitation energy transfer (EET) from the ligand T1 to one or more of the Ln-centered $4f^N$ excited states (^5D_J, J = 4–0), (4) internal conversion (IC) from the ^5D_J state to the lowest quintet state ($^5D_4$), and (5a) green emission via the f–f transitions. The mechanism of quenching of Tb complexes can also be explained based on Figure 1.[10,12,20] After the process (4), the lifetime of the $^5D_4$ state is rather long because the f–f transitions from $^5D_4$ to ^7F_J are parity- and spin-forbidden transitions. Therefore, if the reaction barrier of backward EET from (S0, $^5D_4$) to (T1, $^7F_6$) (5b) is not too high, the backward EET process takes place, and the intensity of the green emission (5a) decreases as temperature increases. To determine the reaction barrier of the complete backward process from (S0, $^5D_4$) to (S0, $^7F_6$), the barriers of two individual steps must be determined: the lowest crossing point between (S0, $^5D_4$) and (T1, $^7F_6$) (5b) and the lowest crossing point for ISC between (T1, $^7F_6$) and (S0, $^7F_6$)

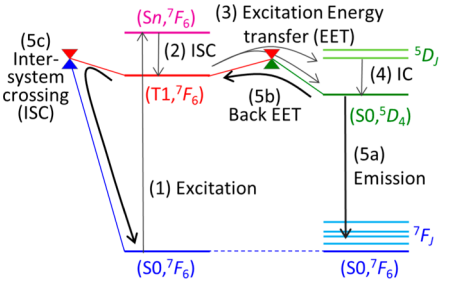

Figure 1. Possible mechanism of Tb^{3+} luminescence and quenching.

Received: July 25, 2014

   dx.doi.org/10.1021/ct500668n | J. Chem. Theory Comput. XXXX, XXX, XXX–XXX

(5c). To design an appropriate temperature sensor, the energies of these minima and crossing points need to be controlled.

To better understand the mechanism and rationally design ligands, theoretical investigations are indispensable. However, *ab initio* calculations for excited states of Ln compounds are highly demanding because relativistic effects, especially spin−orbit interaction, and electron correlation need to be considered explicitly.[6,7] In addition, the structural flexibility around Ln results in the existence of a number of local minima (LM), transition states (TSs), and crossing points between PESs; thus, exhaustive sampling of structures is often required.[21] Due to these difficulties, there has not been a theoretical study in which crossing points between PESs were determined in order to discuss the forward and backward EETs in Ln complexes. In previous studies, the rate of EET has been discussed only on the basis of crystal field theory[22−26] or by comparing the experimental $4f^N$ excitation energy levels with the computed ligand-localized excitation energy levels.[27−34] In most theoretical[22,23,25,27−34] and experimental[12,17,20,35−38] studies, the efficiency of EET has been estimated by considering it to be correlated with the energy gap between the lowest triplet T1 state of the ligand and the excited state of Ln^{3+}.

To overcome these problems, we propose the energy shift method, a reasonable approximation to describe the PESs and to find the crossing points related to the emission and quenching. As mentioned above, the PESs of $4f^N$ excited states have nearly identical shapes to that of the $4f^N$ ground state, and the excitation energies are independent of the environment.[4−7] Therefore, the PESs of $4f^N$ excited states can be described by that of the $4f^N$ ground state corrected by an "energy shift" that is unique for each excited state. For example, the PES of the $^5D_4$ state in a Tb^{3+} complex can be described by that of the $^7F_6$ state with an energy shift, 58.6 kcal/mol, that is equal to the experimental energy difference Δ ($^5D_4$ - $^7F_6$) between $^5D_4$ and $^7F_6$,[10] as shown in Figure 2. When Tb^{3+} is surrounded by

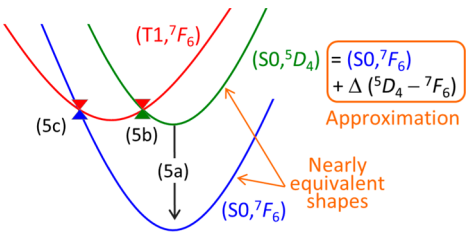

Figure 2. Schematic illustration of PESs involved in the emission and quenching in a Tb^{3+} complex. The states (S0, $^5D_4$), (T1, $^7F_6$), and (S0, $^7F_6$), as well as the notation (5a-c), are the same as those shown in Figure 1.

ligands, the ^SL_J level consisting of $2J + 1$ states becomes nondegenerate. However, such crystal field splittings are typically much smaller than spin−orbit splittings[1−7] and can usually be ignored in qualitative discussions. Therefore, for the three states in Figure 2, only the lowest singlet (S0) and the lowest triplet (T1) states need to be calculated explicitly. These lowest state PESs can be calculated without explicitly considering 4f electrons by the use of a relativistic effective core potential (RECP)[39,40] in a conventional DFT calculation, instead of using highly demanding *ab initio* calculations. An advantage of this approximation is the low computational cost, which enables us to perform an exhaustive exploration of LM, TSs, and crossing points for all internal degrees of freedom on and between PESs of large molecular systems.

As the first case study, we apply this method to three Tb^{3+} complexes containing different anionic ligands; hexafluoroacetylacetonato (hfa), acetylacetonate (acac), and nitrate ion (NO_3^-). According to the experimental studies,[10−12,15,41] the emission intensities of $Tb(X)_3(H_2O)_2$ (X = hfa and acac) *decrease* as the temperature increases, and the change of intensity for X = hfa is larger than that for X = acac. The Gibbs free energies of reaction barriers for the quenching have also been estimated[41] by the observed lifetimes, as 12.5 and 15.5 kcal/mol, for X = hfa and acac, respectively at 298 K.[10] In contrast, the intensity of $Tb(NO_3)_3$ slightly *increases* as the temperature increases.[10,12,15,41] The reason for the different behaviors of the three complexes has not been clarified.

To explain the ligand dependence of the thermosensitivity, the critical points on and between the PESs were determined for the three Tb complexes, $Tb(X)_3(H_2O)_2$ (X = hfa, acac, NO_3^-). We focus on two minimum energy crossing points (MEXs) between the PESs. The one between (T1, $^7F_6$) and (S0, $^5D_4$) was calculated from the lowest triplet state (T1) and the lowest singlet state (S0) of the complex after taking into account the energy shift Δ ($^5D_4$ - $^7F_6$). This MEX corresponds to the point where forward and backward EETs (5b) are most likely to take place. The other MEX is between (T1, $^7F_6$) and (S0, $^7F_6$), calculated as the lowest triplet and the lowest singlet state, respectively, of the complex. This represents the MEX where ISC within the ligand, i.e. quenching (5c), is most likely to take place. The lowest singlet and lowest triplet states were calculated with the dispersion-corrected B3LYP-D3 theory,[42−44] and the full geometry optimizations of LM and MEXs[45−47] were performed using the Global Reaction Root Mapping (GRRM) program[48] with energies and energy derivatives computed by the Gaussian09 program.[49] The GRRM strategy with a model function allows efficient determination of MEXs without needing their approximate locations, which are difficult to guess.[45−47] The structures of (T1, $^7F_6$) LM were used as initial structures for the search and optimization of nearby MEXs. Tb^{3+} was described by using the large-core RECP method in which eight 4f electrons were included in the RECP and only the valence 5s, 5p, 5d, and 6s electrons were calculated explicitly.[39,40] The basis sets were the (7s5p5d)/[5s4p3d] RECP basis set for Tb^{3+}[39,40] and cc-pVDZ for others. As discussed above, the experimental excitation energy Δ ($^5D_4$ - $^7F_6$) of 58.6 kcal/mol[10] was used for the energy shift value. All the connectivity between MEX and LM were confirmed by the intrinsic reaction coordinate (IRC) analysis.[50]

Figure 3 shows the energies of the obtained LM and MEXs for the three complexes. Of the three $Tb(X)_3(H_2O)_2$ complexes, X = hfa has the lowest (T1, $^7F_6$) LM energy of −0.1 kcal/mol with respect to the (S0, $^5D_4$) LM. The complexes with acac and NO_3^- have higher energies of 10.3 and 6.1 kcal/mol, respectively. For the forward EET process (3) from (T1, $^7F_6$) to (S0, $^5D_4$), there could be two pathways. The first is via the direct EET from (T1, $^7F_6$) to (S0, $^5D_4$). The second is through the EET from (T1, $^7F_6$) to a higher state (S0, $^5D_3$), followed by the IC from (S0, $^5D_3$) to (S0, $^5D_4$). However, the relative energy of the (S0, $^5D_3$) LM is 16.7 kcal/mol, higher than the (S0, $^5D_4$)/(T1, $^7F_6$) MEX for all three complexes. Therefore, the forward as well as backward EET should proceed directly through the (S0, $^5D_4$)/(T1, $^7F_6$) MEX without mediation of (S0, $^5D_3$).

dx.doi.org/10.1021/ct500668n | J. Chem. Theory Comput. XXXX, XXX, XXX−XXX

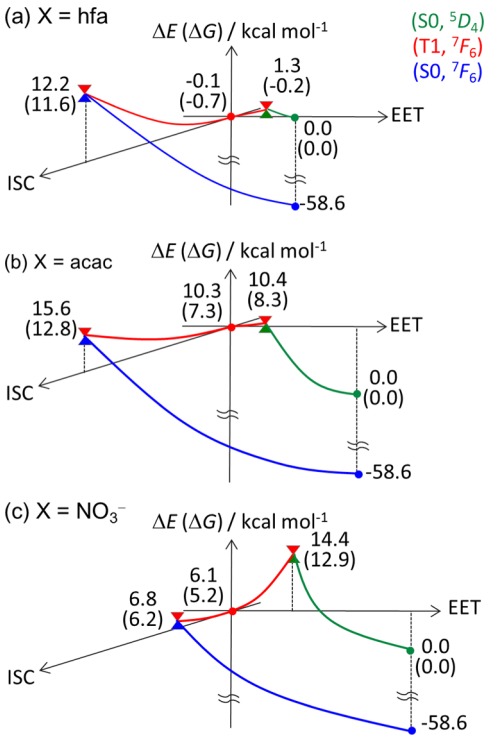

Figure 3. Energies of LM and MEXs on and between PESs, respectively, for $Tb(X)_3(H_2O)_2$ complexes (X = (a) hfa, (b) acac, and (c) NO_3^-). Green curve: (S0, $^5D_4$); red: (T1, $^7F_6$); blue: (S0, $^7F_6$). The relative electronic energies (values in parentheses are the Gibbs free energy difference at 298 K) are in kcal/mol. Two active coordinates, one for EET and the other for ISC, are also depicted.

For $Tb(hfa)_3(H_2O)_2$, the energies of (S0, $^5D_4$) LM (0 kcal/mol, reference) and (T1, $^7F_6$) LM (−0.1 kcal/mol) are nearly identical, as shown in Figure 3(a). Their geometries are also similar, as shown in Figure 4(a). The (S0, $^5D_4$)/(T1, $^7F_6$) MEX between these states also has a quite similar structure and energy (1.3 kcal/mol), meaning that the forward and backward EETs proceed nearly without barriers. The highest point in the quenching process is the (S0, $^7F_6$)/(T1, $^7F_6$) MEX, 12.2 kcal/mol, where the ISC occurs. Therefore, the rate-determining step for quenching is the ISC, not the EET. The excitation is localized on the bent hfa ligand, which is confirmed by the spin density shown in Figure S1. Ligand-localized excitation has also been found for other Ln complexes in previous theoretical calculations.[27−29,31,34] Several important structural parameters are listed in Table S1. The structure of this ISC MEX (in yellow in Figure 4 (b)(i)) is similar to those of other LM and MEXs except one hfa ligand has a bent structure at this MEX. The reaction coordinate to reach this ISC MEX from (T1, $^7F_6$) LM is C−O bending coupled with Tb−O and C−O stretches, as shown in Table S1. The structural and energetic changes can be understood in part based on the isolated hfa ligand, as shown in Figure S2; both singlet and triplet LM have planar structures, while the ISC MEX has a C−O bent structure with longer C−O distance. The relative energies of the T1 LM and the ISC MEX (T1/S0) of the isolated ligand are similar to those in $Tb(hfa)_3(H_2O)_2$, although there are small differences due to the coordination of Tb^{3+}.

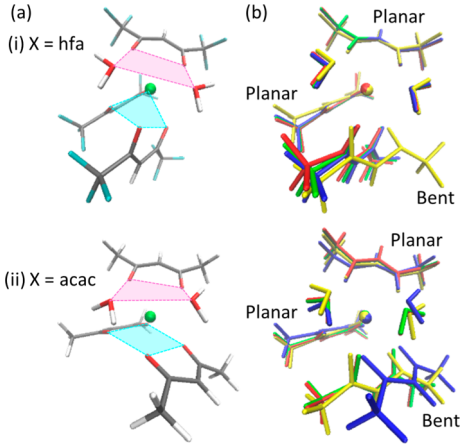

Figure 4. (a) The geometries of LM on (S0, $^5D_4$) with square antiprism structures and (b) comparison of four critical points in $Tb(X)_3(H_2O)_2$ (X = hfa and acac); blue: (S0, $^5D_4$) LM; red: (T1, $^7F_6$) LM; green: (S0, $^5D_4$)/(T1, $^7F_6$) EET MEX; and yellow: (S0, $^7F_6$)/(T1, $^7F_6$) ISC MEX.

The PES of $Tb(acac)_3(H_2O)_2$ is similar to that of $Tb(hfa)_3(H_2O)_2$. The highest energy point for the quenching process is the (S0, $^7F_6$)/(T1, $^7F_6$) ISC MEX at 15.6 kcal/mol, rather than the (S0, $^5D_4$)/(T1, $^7F_6$) backward EET MEX at 10.4 kcal/mol, as shown in Figure 3(b). The reaction coordinate for the ISC is C−O bending coupled with Tb−O and C−O stretches, which is similar to that of $Tb(hfa)_3(H_2O)_2$, as shown in Table S2. The excitation is localized on one acac ligand that has a bent structure, as shown in Figure 4(b). The major difference between $Tb(acac)_3(H_2O)_2$ and $Tb(hfa)_3(H_2O)_2$ is that the (T1, $^7F_6$) LM is 10.3 kcal/mol higher than the (S0, $^5D_4$) LM reference. Since the EET MEX is close to the (T1, $^7F_6$) LM both in terms of energy and structure, the forward EET proceeds without a barrier. However, the backward EET with a 10.4 kcal/mol barrier should proceed more slowly than for $Tb(hfa)_3(H_2O)_2$, where backward EET had a very low barrier. The high energy and bent structure can also be seen in the isolated acac ligand, as shown in Figure S2. The difference in the T1 LM structures between hfa and acac can be attributed to the electronegativity. The hfa ligand has electron-withdrawing groups, CF_3, that allow the negative charge to be delocalized, stabilizing the structure, whereas the acac ligand has an electron-donating group, CH_3, causing the negative charge to be localized on two C−O bonds, which results in a bent structure that reduces the electron repulsion. Comparing the Gibbs free energies of the ISC MEXs for $Tb(X)_3(H_2O)_2$ (X = hfa and acac), that for X = hfa (11.6 kcal/mol) is lower than that for X = acac (12.8 kcal/mol), which is consistent with the experimental barriers for quenching of 12.5 and 15.5 kcal/mol.[41] Although these barriers estimated by experimental lifetimes[41] might include the effect of the (T1, $^7F_6$)/(S0, $^7F_6$) nonadiabatic transition probability not included in our calculations, we qualitatively reproduced the relative barrier heights for quenching. Note that there are several conformers for $Tb(X)_3(H_2O)_2$ in which the position of two water molecules are different, as shown in Figure S3. The energies of (S0, $^5D_4$) LM and (T1, $^7F_6$) LM were compared for different conformers. Their energy differences are less than 1.5 kcal/mol, and the most stable conformers of (S0, $^5D_4$) and (T1, $^7F_6$), which we adopted, are the same. The conformational change does not take place during the emission and quenching process.

The dependence of the emission intensity on the temperature for $Tb(X)_3(H_2O)_2$ (X = hfa and acac) can be explained by

dx.doi.org/10.1021/ct500668n | J. Chem. Theory Comput. XXXX, XXX, XXX−XXX

the features of the PESs. For the emission process, the forward EET proceeds without a barrier, and thus the rate is determined by the f−f transition probability, which is independent of the temperature. By contrast, for quenching, the rate is determined by the barrier of the ligand-centered ISC through the (S0,$^7F_6$)/(T1,$^7F_6$) MEX. Therefore, as temperature increases, the rate of quenching increases and the emission intensity decreases. In addition, it can be understood that the emission intensity decrease is more prominent for X = hfa than X = acac because of the lower quenching barrier for the former.

For $Tb(NO_3)_3(H_2O)_2$, there are two conformers in which two water molecules are in *cis* or *trans* positions, as shown in Figure S4. The energy and geometry of the most stable *trans* conformer are shown in Figures 3(c) and 5, respectively. The

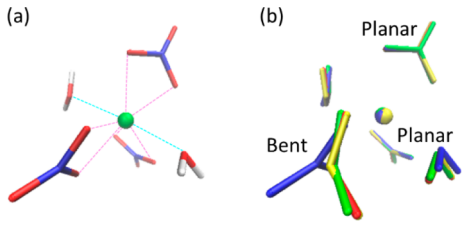

Figure 5. (a) The geometries of LM on (S0, $^5D_4$) and (b) comparison of four critical points in $Tb(NO_3)_3(H_2O)_2$ in which two H_2O are in *trans* positions; blue: (S0, $^5D_4$) LM; red: (T1, $^7F_6$) LM; green: (S0, $^5D_4$)/(T1, $^7F_6$) EET MEX; and yellow: (S0, $^7F_6$)/(T1, $^7F_6$) ISC MEX.

excitation is localized on one NO_3^- ligand as shown in Figure S1, and its structure changes from planar to pyramidal for (T1, $^7F_6$) LM and MEXs as shown in Figure 5. The same structural change also occurs for the isolated NO_3^-, as shown in Figure S2. Although there are some similarities among the three Tb complexes, the features of the PESs for $Tb(NO_3)_3(H_2O)_2$ are quite different from the others. The most notable difference is that the highest energy point is not the (S0, $^7F_6$)/(T1, $^7F_6$) ISC MEX at 6.8 kcal/mol but the (S0, $^5D_4$)/(T1, $^7F_6$) EET MEX at 14.4 kcal/mol, as shown in Figure 3(c). Thus, forward as well as backward EET have relatively high barriers. The reason for the increase in emission intensity for increased temperature can be understood by this MEX. The rate-determining step is the (S0, $^5D_4$)/(T1, $^7F_6$) EET both for emission and quenching, and the barrier for forward EET, leading to emission, is much lower than that for backward. Therefore, the emission intensity increases with temperature. Although the calculated PESs predict competition between the forward EET and the ISC, the rate for the (S0, $^7F_6$)/(T1, $^7F_6$) ISC is almost independent of the temperature and does not affect the temperature sensitivity.

As shown above, the origin of the temperature dependence of the emission intensity is not the same for all Tb complexes. The efficiency of forward and backward EETs for $Tb(X)_3(H_2O)_2$ (X = hfa and acac) can be understood very qualitatively by the energy difference between (S0, $^5D_4$) and (T1, $^7F_6$) as discussed in previous theoretical[22,23,25,27−34] and experimental[12,17,20,35−38] studies of various Ln compounds. However, the EET efficiencies for X = NO_3^- and the influence of the ISC can only be explained by the energy levels of the MEXs. The most notable advantage of the present energy shift approach is that the structures of MEXs and LM can be fully optimized. The reaction coordinates for EET and ISC can be determined without bias and at relatively low computational cost. Therefore, this strategy can be used in exhaustive searches for MEXs considering all possible conformers and reaction coordinates, which would enable the computational design of appropriate Ln complexes for luminescence sensors. Additionally, the obtained geometries can be used for highly accurate *ab initio* calculations of transition probabilities, enabling accurate predictions of the rates and lifetimes of emission and quenching. We are currently investigating the PESs of the Tb complexes using a highly accurate *ab initio* method with 4f electrons treated explicitly to test our approach, and the results will be reported in due course.

■ ASSOCIATED CONTENT

Ⓢ Supporting Information

Spin density maps of the triplet states, structural parameters, PESs of isolated ligands, structures and energy levels of different conformers, critical points on and between PESs for $Tb(NO_3)_3$, and Cartesian coordinates and absolute energies. This material is available free of charge via the Internet at http://pubs.acs.org.

■ AUTHOR INFORMATION

Corresponding Authors

*E-mail: miho@fukui.kyoto-u.ac.jp (M.H.).
*E-mail: morokuma@fukui.kyoto-u.ac.jp (K.M.).

Notes

The authors declare no competing financial interest.

■ ACKNOWLEDGMENTS

The authors are grateful to Dr. Travis Harris of State University of New York at Oswego for his help in improving the paper and Prof. Satoshi Maeda of Hokkaido University for his GRRM code and discussions on the GRRM method. This work was partly supported by Grants-in-Aid from MEXT for Innovative Areas (Soft Molecular Systems, No. 26104519), for Young Scientist (B) (No. 26810005) to M.H. and for Scientific Research (A) (No. 24245005) to K.M. at Kyoto University. M.H. acknowledges the Fukui Fellowship of Kyoto University and Collaborative Research Program for Young Scientists of ACCMS and IIMC, Kyoto University. The Computer resources at the Academic Center for Computing and Media Studies (ACCMS) at Kyoto University and Research Center of Computer Science (RCCS) at the Institute for Molecular Science are also acknowledged.

■ REFERENCES

(1) Eliseeva, S. V.; Bünzli, J.-C. G. *Chem. Soc. Rev.* **2010**, *39*, 189−227.
(2) Binnemans, K. *Chem. Rev.* **2009**, *109*, 4283−4374.
(3) Bünzli, J.-C. G.; Piguet, C. *Chem. Soc. Rev.* **2005**, *34*, 1048−1077.
(4) Bünzli, J.-C. G.; Eliseeva, S. V. In *Lanthanide Luminescence: Photophysical, Analytical and Biological Aspects*; Hänninen, P., Härmä, H., Eds.; Springer Ser Fluoresc: Amsterdam, 2010; Vol. 7, p 1−46.
(5) Hasegawa, Y.; Wada, Y.; Yanagida, S. *J. Photochem. Photobiol., C* **2004**, *5*, 183−202.
(6) Hatanaka, M.; Yabushita, S. *J. Phys. Chem. A* **2009**, *113*, 12615−12625.
(7) Hatanaka, M.; Yabushita, S. *Theor. Chem. Acc.* **2014**, *133*, 1517−1531.
(8) Buddhudu, S.; Morita, M.; Murakami, S.; Rau, D. *J. Lumin.* **1999**, *83−84*, 199−203.
(9) Mitsuishi, M.; Kikuchi, S.; Miyashita, T.; Amao, Y. *J. Mater. Chem.* **2003**, *13*, 2875−2879.
(10) Katagiri, S.; Hasegawa, Y.; Wada, Y.; Yanagida, S. *Chem. Lett.* **2004**, *33*, 1438−1439.

(11) Katagiri, S.; Hasegawa, Y.; Wada, Y.; Mitsuo, K.; Yanagida, S. *J. Alloys Compd.* **2006**, *408*−*412*, 809−812.
(12) Katagiri, S.; Tsukahara, Y.; Hasegawa, Y.; Wada, Y. *Bull. Chem. Soc. Jpn.* **2007**, *80*, 1492−1503.
(13) Yu, J.; Sun, L.; Peng, H.; Stich, M. I. J. *J. Mater. Chem.* **2010**, *20*, 6975−6981.
(14) Peng, H.; Stich, M. I. J.; Yu, J.; Sun, L.; Fischer, L. H.; Wolfbeis, O. S. *Adv. Mater.* **2010**, *22*, 716−719.
(15) Miyata, K.; Konno, Y.; Nakanishi, T.; Kobayashi, A.; Kato, M.; Fushimi, K.; Hasegawa, Y. *Angew. Chem., Int. Ed.* **2013**, *52*, 6413−6416.
(16) Yuasa, J.; Mukai, R.; Hasegawa, Y.; Kawai, T. *Chem. Commun.* **2014**, *50*, 7937−7940.
(17) Crosby, G. A.; Whan, R. E.; Alire, R. M. *J. Chem. Phys.* **1961**, *34*, 743−748.
(18) Whan, R. E.; Crosby, G. A. *J. Mol. Spectrosc.* **1962**, *8*, 315−327.
(19) Kleinerman, M. *J. Chem. Phys.* **1969**, *51*, 2370−2381.
(20) Sato, S.; Wada, M. *Bull. Chem. Soc. Jpn.* **1970**, *43*, 1955−1962.
(21) Hatanaka, M.; Maeda, S.; Morokuma, K. *J. Chem. Theory Comput.* **2013**, *9*, 2882−2886.
(22) de Sá, G. F.; Malta, O. L.; Donega, C. D.; Simas, A. M.; Longo, R. L.; Santa-Cruz, P. A.; da Silva, E. F. *Coord. Chem. Rev.* **2000**, *196*, 165−195.
(23) Gonçalves e Silva, F. R.; Longo, R. L.; Malta, O. L.; Piguet, C.; Bünzli, J.-C. G. *Phys. Chem. Chem. Phys.* **2000**, *2*, 5400−5403.
(24) Malta, O. L. *J. Non-Cryst. Solids* **2008**, *354*, 4770−4776.
(25) Faustino, W. M.; Nunes, L. A.; Terra, I. A. A.; Felinto, M. C. F. C.; Brito, H. F.; Malta, O. L. *J. Lumin.* **2013**, *137*, 269−273.
(26) Dutra, J. D.; Bispo, T. D.; Freire, R. O. *J. Comput. Chem.* **2014**, *35*, 772−775.
(27) Gutierrez, F.; Tedeschi, C.; Maron, L.; Daudey, J.-P.; Poteau, R.; Azema, J.; Tisnès, P.; Picard, C. *Dalton Trans.* **2004**, 1334−1347.
(28) Gutierrez, F.; Tedeschi, C.; Maron, L.; Daudey, J.-P.; Poteau, R.; Azema, J.; Tisnès, P.; Picard, C.; Poteu, R. *J. Mol. Struct.: THEOCHEM* **2005**, *756*, 151−162.
(29) Gutierrez, F.; Rabbe, C.; Poteu, R.; Daudey, J. P. *J. Phys. Chem. A* **2005**, *109*, 4325−4330.
(30) Aiga, F.; Iwanaga, H. Amano. *J. Phys. Chem. A* **2005**, *109*, 11312−11316.
(31) Guillaumont, D.; Bazin, H.; Benech, J.-M.; Boyer, M.; Mathis, G. *ChemPhysChem* **2007**, *8*, 480−488.
(32) Li, X.-N.; Wu, X.-J.; Si, Z.-J.; Zhou, L.; Liu, X.-J.; Zhang, H.-J. *Phys. Chem. Chem. Phys.* **2009**, *11*, 9687−9695.
(33) Puntus, L. N.; Lyssenko, K. A.; Pekareva, I. S.; Bünzli, J.-C. G. *J. Phys. Chem. B* **2009**, *113*, 9265−9277.
(34) Freidzon, A. Y.; Scherbinin, A. V.; Bagaturyants, A. A.; Alfimov, M. V. *J. Phys. Chem. A* **2011**, *115*, 4565−4573.
(35) Latva, M.; Takalo, H.; Mukkala, V.-M.; Matachescu, C.; Rodríguez-Ubis, J. C.; Kankare, J. *J. Lumin.* **1997**, *75*, 149−169.
(36) Archer, R. D.; Chen, H.; Thompson, L. C. *Inorg. Chem.* **1998**, *37*, 2089−2095.
(37) Hasegawa, M.; Ishii, A.; Kishi, S. *J. Photochem. Photobiol., A* **2006**, *178*, 220−224.
(38) Kachi-Terajima, C.; Yanagi, K.; Kaziki, T.; Kitazawa, T.; Hasegawa, M. *Dalton Trans.* **2011**, *40*, 2249−2256.
(39) Dolg, M.; Stoll, H.; Savin, A.; Preuss, H. *Theor. Chim. Acta* **1989**, *75*, 173−194.
(40) Dolg, M.; Stoll, H.; Preuss, H. *Theor. Chim. Acta* **1993**, *85*, 441−450.
(41) Katagiri, S. Photosensitized Luminescence Systems of Lanthanide(III) Complexes Showing Temperature-Dependence. Ph.D. Thesis, University of Osaka, March, 2007.
(42) Lee, C. T.; Yang, W. T.; Parr, R. G. *Phys. Rev. B* **1988**, *37*, 785−789.
(43) Becke, A. D. *J. Chem. Phys.* **1993**, *98*, 5648−5652.
(44) Grimme, S.; Antony, J.; Ehrlich, S.; Krieg, H. *J. Chem. Phys.* **2010**, *132*, 154104−154119.
(45) Maeda, S.; Ohno, K.; Morokuma, K. *J. Phys. Chem. A* **2009**, *113*, 1704−1710.
(46) Maeda, S.; Ohno, K.; Morokuma, K. *Adv. Phys. Chem.* **2012**, *2012*, 268124−268136.
(47) Maeda, S.; Ohno, K.; Morokuma, K. *J. Chem. Theory Comput* **2010**, *6*, 1538−1545.
(48) Maeda, S.; Osada, Y.; Morokuma, K.; Ohno, K. *GRRM*, a developmental version at Hokkaido University. The energy shift was made by an interface code which modifies energy obtained by Gaussian09 and gives the modified values to GRRM.
(49) Frisch, M. J.; Trucks, G. W.; Schlegel, H. B.; Scuseria, G. E.; Robb, M. A.; Cheeseman, J. R.; Scalmani, G.; Barone, V.; Mennucci, B.; Petersson, G. A.; Nakatsuji, H.; Caricato, M.; Li, X.; Hratchian, H. P.; Izmaylov, A. F.; Bloino, J.; Zheng, G.; Sonnenberg, J. L.; Hada, M.; Ehara, M.; Toyota, K.; Fukuda, R.; Hasegawa, J.; Ishida, M.; Nakajima, T.; Honda, Y.; Kitao, O.; Nakai, H.; Vreven, T.; Montgomery, J. A.; Peralta, J. E.; Ogliaro, F.; Bearpark, M.; Heyd, J. J.; Brothers, E.; Kudin, K. N.; Staroverov, V. N.; Kobayashi, R.; Normand, J.; Raghavachari, K.; Rendell, A.; Burant, J. C.; Iyengar, S. S.; Tomasi, J.; Cossi, M.; Rega, N.; Millam, J. M.; Klene, M.; Knox, J. E.; Cross, J. B.; Bakken, V.; Adamo, C.; Jaramillo, J.; Gomperts, R.; Stratmann, R. E.; Yazyev, O.; Austin, A. J.; Cammi, R.; Pomelli, C.; Ochterski, J. W.; Martin, R. L.; Morokuma, K.; Zakrzewski, V. G.; Voth, G. A.; Salvador, P.; Dannenberg, J. J.; Dapprich, S.; Daniels, A. D.; Farkas, Ö.; Foresman, J. B.; Ortiz, J. V.; Cioslowski, J.; Fox, D. J. *Gaussian 09*, Revision D.01; Gaussian Inc.: Wallingford, CT, 2009.
(50) Fukui, K. *Acc. Chem. Res.* **1981**, *14*, 363−368.